Heliyon 6 (2020) e04077

Contents lists available at ScienceDirect

Heliyon

journal homepage: www.cell.com/heliyon

Research article

Investigation of FSSW parameters on shear fracture load of AA6061 and copper alloy joints

S. Manickam [a], C. Rajendran [b,*], V. Balasubramanian [a]

[a] Center for Materials Joining and Research (CEMAJOR), Faculty of Engineering and Technology, Annamalai University, Annamalai Nagar, Tamilnadu 608002, India
[b] Department of Mechanical Engineering, Sri Krishna College of Engineering and Technology, Coimbatore, Tamilnadu 641008, India

ARTICLE INFO

Keywords:
Mechanical engineering
Materials science
Materials application
Materials characterization
Materials processing
Materials structure
FSSW
AA6061
Copper alloy
Shear fracture load
Microstructure
Dissimilar joint

ABSTRACT

In this research, Friction stir spot welding (FSSW) is extensively employed to join dissimilar metals consisting of AA6061-T6 Aluminium Alloy and Commercial Copper Alloy. These alloys were friction stir spot welded using process parameters with the major impact, such as Dwell Time (DT), Rotational Speed (RS), Plunge Rate (PR) and Tool Diameter Ratio (D/d). Trail experiments have been carried out using Design of Experiments. Sound welded joints exhibiting a maximum shear fracture load of 4.79 kN were obtained at a RS of 2000 rpm, PR of 7 mm/min, DT of 25 s and D/d of 3.5, Balanced material flow around the pin was also observed at this condition, and it is evident that the superior metallurgical properties and geometric features at this condition results in the higher strength. Moreover, the joint also exhibited higher load-bearing capabilities due to an optimal hook height of 0.89 mm, hook width of 1.3 mm and hook initiation distance of 1.4 mm. The continuous formation of intermetallic compound such as γ_2-Cu_9Al_4 in the Cu zone and η_2-CuAl in the Al zone may also enhance the shear fracture load.

1. Introduction

Aluminum Alloys like AA6061-T6 and Commercial Copper Alloys have been used extensively in aircraft and automobile industries, due to their excellent strength, high corrosion-resistance, good formability and easy machinability. However, these alloys also present huge challenges in both design and welding, as the wide difference in melting points of aluminium and copper limits the use of conventional fusion welding process. So, these dissimilar joints are fabricated by riveting. The riveting process requires tools, additional fixtures, skilled labor, and, also, increases the weight of the joints. Friction Stir Spot Welding (FSSW) is used to join aluminium to aluminum, aluminium to magnesium, aluminium to copper, and aluminium to carbon steel [1, 2, 3, 4, 5, 6, 7, 8]. FSSW has also been employed extensively in the fabrication of body panels in automobiles, and has been found to be efficient in welding aluminium and copper in aluminium car bodies [9]. The Aluminium body sections on the Mazda RX-8 have been fabricated using FSSW [10]. Mazda has been using the FSSW process to link up an aluminum trunk lid to steel hinges in its MX-5 sports car since 2006. The deck lid and hood of the Prius hybrid vehicles manufactured by Toyota are also fabricated using FSSW [11]. FSSW is being used in Japan by Kawasaki Heavy industries to weld the aluminum chassis and sheet panels in the prototype rail cars for the Magnetically-levitated linear motor trains and the next generation bullet trains. A load-controlled process was employed by Sakano et al [12] in joining 1mm thick plates of 6xxx aluminum to obtain an average TSFL of 2.017 kN which was found to be much higher than that obtained through Electrical Resistance Spot Welding (ERSW). It was also found that the strength was dependent on the applied force, the rotational speed and the process time. Kumagai et al [13] performed continuous welds of about 70 joints found using FSSW on 1mm/1 mm thick 6xxx series aluminum using a tool shoulder diameter of 13 mm and observed a better consistency as compared to ERSW. They also reported that the strength obtained at 4 kN was also almost double that of ERSW. A load control process was used by Fujimoto et al [14] to lap weld of 1mm 6xxx series aluminum for a lap shear failure load of 2.6 kN in FSSW. They also studied the variation in the tool penetration depth and lap-shear strength for various process times. The weldability of 0.94mm 6111-T4 aluminum sheets for different pre-determined plunge depths was studied by Pan et al [15] in the failure of lap-shear joints, and they reported a strength of over 3 kN at a1.8 mm depth. Shear failure loads of about 4 kN was found for FSSW joints of 1mm thick 6111-T4 joints and of 3.7 kN for 1 mm thick 5052-H32 joints by Chun et al [16].

* Corresponding author.
E-mail address: crdrn12@yahoo.com (C. Rajendran).

https://doi.org/10.1016/j.heliyon.2020.e04077
Received 21 December 2019; Received in revised form 31 March 2020; Accepted 22 May 2020

Table 1. Chemical composition (%wt.) of selected base materials.

Elements	Mn	Si	P	Al	Mg	Cr	Ni	Cu	Fe
AA6061	0.14	0.4	–	95.7	0.7	0.03	–	0.34	0.71
Cu alloy	–	–	0.02	–	–	–	0.27	90.74	0.027

It is evident from the literature review, that an advance in FSSW has made it possible to use it in the place of riveting and mechanical locking. The effect of FSSW parameters for joining similar alloys, especially aluminum alloys and magnesium alloys has been investigated earlier. But, sufficient published literature is not available on the studies made on FSSW of bimetallic joints using aluminum alloys and copper alloys. Hence, the focus of this investigation is on the effectiveness of FSSW in joining AA6061 aluminum alloy with copper alloy and analyzes the effect of process parameters on shear strength of FSSW joints.

2. Experimental work

Hot rolled AA6061-T6 Aluminium and Commercial Copper Alloy have been used in this investigation. The chemical composition of the base materials was obtained using a vacuum spectrometer method. The spectrum, obtained by igniting sparks at various positions, was analyzed for the estimation of alloying elements of the Base Metal (BM) samples. Tables 1 and 2 respectively present the calculated value of the chemical composition obtained. BM in as received condition was shown to have coarse and elongated grains parallel to the rolling direction (Figure 1a, b). Also, the microstructure of BM was obtained using Scanning Electron Microscope to analyze the grain morphology (Figure 1c, d). "Do-All" machine was used to prepare test samples. Fine grain sandpaper (1000 grits) was used for the initial cleaning process. The FSSW joints was welded using a 4000 rpm, 22kW, 6 ton, CNC Friction Welding machine (Figure 2b). The joints were as per the dimensions shown in Figure 2a. Figure 2c shows the fabricated tool with different shoulder and pin diameter. FSSW parameters such as rotational speed (RS), dwell time (DT), plunge rate (PR) and tool diameter ratio (D/d), were chosen from the previous works and trials. Four factor five level central rotatable composite designs were used to fabricate the joints. The feasible working range was initially fixed for each process parameters (Table 3). This was done by varying one of the FSSW parameters from a minimum to maximum while keeping the other factors. The parameters chosen, the respective ranges used in the investigation, are presented in Table 4.

Thirty joints were fabricated, under different combinations of welding parameters, to study the microstructure and the effect of FSSW parameters on Shear Fracture Load (SFL) (Table 5). Figure 2d, e shows the photograph of bimetallic FSSW joints before and after fracture. The mean value of SFL is shown in Tables 6, 7, 8, and 9. Two joints for lap shear test and one joint for microstructure analysis was made at each condition. The Universal Tensile Machine (FIE-BLUE-STAR) was used with a crosshead velocity of 1.5 kN to calculate SFL. For microstructure analysis, the specimens were sectioned across the transverse cross-section of the weld. After proper polishing, the samples were etched on the AA6061 portion using Keller's reagent and with ferric chloride on the copper to reveal the grain morphology. A light optical microscope, with a provision for image analysis, was used for microscopic analysis (MEJI JAPAN, MIL-7100 with Meta vision). Hardness was studied using a Vicker microhardness tester (Make Shimaduz and Model: HMV-2T). The fracture patterns were analyzed using a scanning electron microscope (JEOL, JAPAN).

3. Results and discussions

3.1. Effect of rotational speed

Test results shows that RS has a effect on the SFL of joints (Figure 3a-c). SFL of the joints increases with increase in RS from 1600 rpm to 2000 rpm and then decreases upto 2000 rpm. The maximum SFL of 4.79 kN was obtained in the joint fabricated at a RS of 2000 rpm, and the lowest SFL of 2.99 kN was observed in the joint fabricated at a RS of 1600 rpm. From the hardness survey, it is observed that the RS has a perceptible influence on the hardness of the welds. The maximum hardness is found at the vicinity of keyhole, irrespective of the RS used. The interface of thermo-mechanically affected zone (TMAZ) and heat affected zone (HAZ) has the minimum hardness. The nugget zone microhardness

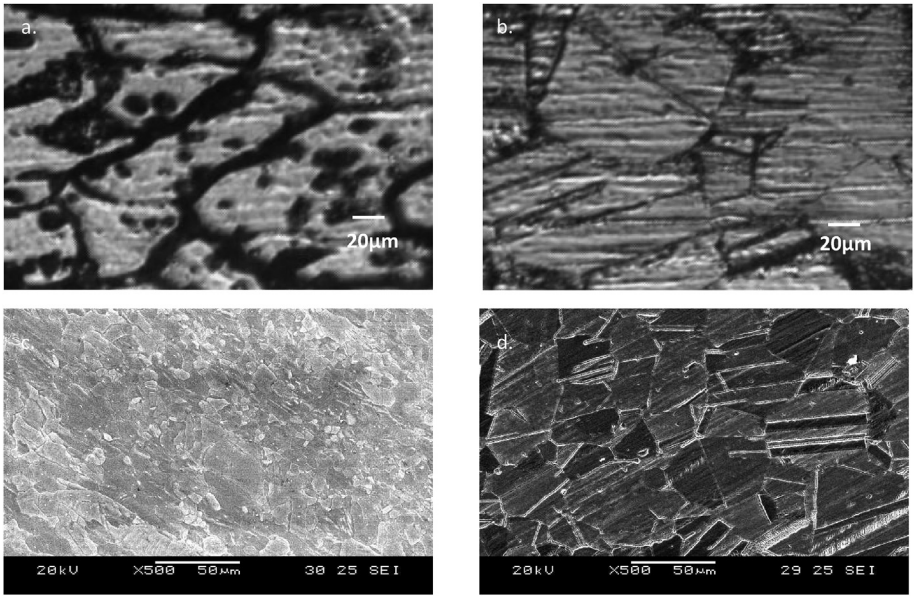

Figure 1. Micrograph of a) AA6061 b) Cu alloy, SEM micrograph of c) AA6061 and d) Cu alloy.

Table 2. Mechanical properties of selected base materials.

Materials	0.2% Yield Strength (MPa)	Tensile strength (MPa)	Elongation in 50 mm gauge length (%)	Microhardness @0.5 N, 15 s (HV)
AA6061	280	307	15	108
Cu alloy	221	267	27	196

increases with RS from 1600 rpm to 2000 rpm and then reduces with further increase in RS. The highest nugget zone microhardness of 168 HV was noticed in at a RS of 2000 rpm. The lowest nugget zone microhardness of 139 HV was observed at a RS of 1600 rpm.

Figure 4c shows that the RS has a perceptible influence on the grain size found in all the three regions of the weld. The elongated and coarse grains of the BMs are converted into fine equi-axed grains in the nugget zone due to thermal flux. The grains are elongated, inclined and coarser in the TMAZ when compared to the nugget zone in all the welds (Figure 4a-e). The grains are found to be equi-axed in both the HAZ and the nugget zone but larger in the nugget zone. As the RS increases, the grain size decreases in all zones. The nugget zone of the joint fabricated at 2000 rpm consists of extremely fine grains (Figure 4c). The fractured surface was also characterized using SEM to find the failure pattern. Figure 5 shows the photographs of the top and bottom sheet of the joint after testing and SEM fractographs of the tested joints. It is found from the study of the fracture surface, that the RS has a major influence on the mode of failure of the FSSW joints. At a RS of 1600 rpm the joint reveals 'eyelet' mode of failure at the fractured surface, and the fractured surfaces at RS of 1800 rpm, 2200 rpm and 2400 rpm reveal 'Partially Curved' mode of failure. The fractured surface of joint fabricated at a RS of 1000 rpm exhibits 'Nugget Pull out' type of failure (Table 6) (see Figure 6).

It is well established in friction stir welding, that the frictional heat developed is directly proportional to the RS [17]. The variations in temperature during plunging may be due to different contact conditions of tool and material such as sliding, sticking or a combination of sliding and sticking due to the frictional coefficient resulting in momentary changes in local temperatures. Due to the increased RS, the highest temperature reached is increased, which, in turn increases the volume of the nugget zone. Further increase of RS does not substantially increase the volume of the nugget zone. It is clearly shown by Gerlich et al. [18]

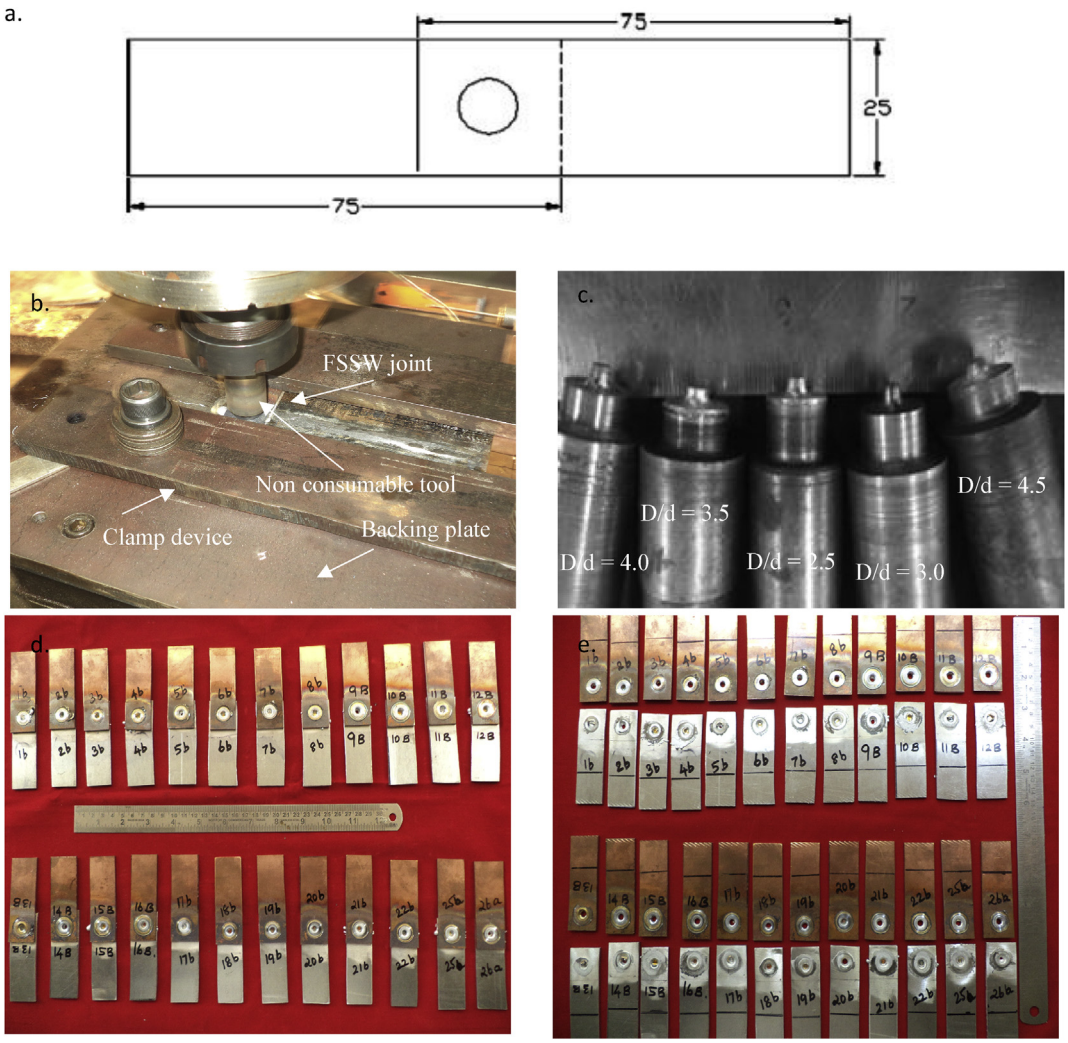

Figure 2. a) Joint configuration [1], Photograph of b) FSSW set up joints, c) Fabricated tool for FSSW, d) FSSW joints (before fracture) and e) FSSW joints (after fracture).

Table 3. Feasible working limit of FSSW of AA6061 with copper alloy joints.

Parameters	Tool rotational speed "rpm"		Plunge rate "mm/min"	
Range	N < 1600	N > 2400	R < 5	R > 9
Probable reasons	Insufficient material flow due to low heat input	More heat input cause distortion	Heat generation low	High rate of plunge leads to key hole defect
Parameters	Dwell time "Sec"		Tool diameter ratio	
Range	T < 15	T > 35	D < 2.5	D > 4.5
Probable reasons	Low heat input results in lack of fill	High dwell time results in key hole and distortion	Insufficient material flow due to low heat input	High heat input and work hardening distortion

that the higher RS had little influence on heat generated as the torque decreases correspondingly, and, that there would be no remarkable change in the nugget zone width and nugget zone volume. At lower RS, the low peak temperature, followed by a faster cooling rate, causes low heat input and low stirring action, which results in a partial recrystallization in the nugget zone. The higher peak temperature at higher RS, followed by the slower cooling rate, causes the formation of coarser grains in the nugget zone.

This phenomenon can also affect the precipitate size and shape. Hence, the optimum temperature, in conjunction with axial force and its duration, formed finer grains in the nugget zone at RS of 2000 rpm. The equi-axed grains found in the nugget zone are due to churning and recrystallization of plasticized material [19]. Liu et al [20] also found the formation of equi-axed grains in the nugget zone of friction stir welding. The excessive heat input is not used to increase the volume of the nugget zone, and only the width of the HAZ is increased instead [21]. Even though the cycle time is same for all the spots, the changes in RS caused a wide-range of churning and mixing of material around the rotating pin and variations in peak temperature generation; the quantity of heat input and the forging force on the sheets to be welded. The axial force is reduced with increase in tool RS, which results in poor material consolidation between top and bottom sheets and causes a reduced region of complete metallurgical bond in the weld nugget [22]. Even though the forging force is higher at lower RS, the insufficient heat generation causes the minimum hardness at the nugget zone. The actual nugget diameter, which is a measure of the size, increases with increasing RS under a given probe length [23]. Since the increase in the actual nugget diameter results in increase of SFL under loading due to the increased effective area.

The geometrical features resulting due to the effect of RS on of symmetrically sectioned specimens of FSSW joints is presented in Table 5. The features of the joint such as hook height (HH), hook width (HW) and hook initiation distance (HI) were recorded from the macrographs. Of the five combinations of RS, the HI and the HW increases to certain extent and then decreases. On the other hand, with increasing RS, the HH decreases to a certain limit and then increases. Since the features of all the joints depend up on the material flow behavior, the flow behavior can be divided into three states i) balanced material flow, ii) in sufficient material flow and iii) turbulent material flow. In this case, low RS (1600 rpm) causes lower agitation due to the threaded pin and results in insufficient material flow. Moreover, the vertical movement of plasticized materials was also observed to be low. Hence the joint yielded low HW and HI value. At higher RS (2400 rpm), the heavier strain on the material in the stirring zone increases the HH. This can be attributed to the turbulent flow of plastic material. Moreover, the effective sheet thickness is also reduced.

3.2. *Effect of plunge rate*

PR is the movement of the tool between the two sheets with respect to time. In this work, a threaded profile on a tapped pin was used. SFL of the joint increases as PR is increased from 5 mm/min to 7 mm/min and then the SFL decreases (Figure 3a, d, e). The highest SFL of 4.79 kN were found in the joint made at a PR of 7 mm/min, and the lowest SFL of 3.79 kN was observed fabricated at a PR of 5 mm/min. The features such as HH, HW, HI, obtained from the macrographs, are presented in Table 6. Also, the increase in HW increases the SFL whereas the increase of HH decreases SFL, irrespective of the PR. HI, with a few exceptions, is found to increase with the increase in SFL. The maximum SFL obtained at a PR of 7 mm/min, possesses the optimum HW and HH of 1.397 mm and 0.326 mm respectively, whereas the lowest SFL, at a PR of 5 mm/min, displays HW and HH of 0.77 mm and 0.87 mm respectively. The maximum hardness is recorded at the vicinity of keyhole, and the minimum hardness is recorded at the interface of TMAZ and HAZ, irrespective of the PR used. The nugget zone microhardness increases with increases in PR from 5 mm/min to 7 mm/min and then decreases with further increase in PR. The highest nugget zone microhardness of 168 HV was

Table 4. Used FSSW parameters and their level.

Sl. No	Factor	Unit	Notation	Levels				
				-2	-1	0	1	2
1	Rotational speed	rpm	RS	1600	1800	2000	2200	2400
2	Plunge rate	mm/min	PR	5	6	7	8	9
3.	Dwell time	sec	DT	15	20	25	30	35
4	Tool diameter ratio	–	D/d	2.5	3.0	3.5	4.0	4.5

obtained a PR of 7 mm/min. The lowest nugget zone microhardness of 145 HV was recorded at a PR of 5 mm/min. The optical micrographs at different PR are shown in Figure 4 (f-j). It is observed from the micrographs that the PR has an influence size of the grains formed in the nugget, TMAZ and HAZ. Very fine grains are found in the nugget at 7 mm/min (Figure 4h). Grain size is slightly coarser in the nugget zone of the joints fabricated at other PR. Fracture surface analysis shows that the fractured surface of the joint at a PR of 5 mm/min and 9 mm/min reveal 'Partially Curved' mode of failure. The fractured surface of the joint fabricated using a PR of 7 mm/min exhibits 'Nugget Pull out' type of failure. The fractured surface of joint fabricated using PR of 6 mm/min and 8 mm/min reveals 'Partially Curved' mode of failure.

The rate of heat input is inversely proportional to the PR, unlike for the other parameters. The cycle time is reduced at higher PR whereas cycle time is increased at lower PR. High peak temperature was recorded at lower PR (5 mm/min), which in turn increases heat input. A coarser grain structure results in the nugget zone due to the excessive mixing action due to the longer cycle times. Moreover, high strained materials may come out in term of flash. The FSSW joint has key hole defect at the bottom sheet strained materials may be expelled as Flash. In contrast, at higher PR (9 mm/min), the flow through the stained materials along the groove is lower due to the low stirring action, causing insufficient material flow and resulting in improper bonding. Hence the SFL of FSSW joint was lower at higher PR. Moreover, the low peak temperature, results in low heat input and inadequate stirring action, leading to a coarser grain structure in the nugget zone. The higher peak temperatures and the longer duration of the axial force results in finer grains in the nugget zone. The reduction of dislocation density and precipitate distribution, when compared to the BM, leads to considerable softening of the material in the nugget zone [24, 25, 26, 27]. The changes in PR also cause the wide-range of churning and mixing of material around the rotating pin, the variations in the peak temperature generation and the forging force on the sheets to be welded. Moreover, the PR is indirectly influenced by the hardness of the material to be welded, which greatly affects the performance of the joints. The incidence of forging force is reduced with increase of higher PR, which results in poor material consolidation

Table 5. Combination of FSSW parameters used to fabricate the bimetallic joints (Based on design matrix).

Exp. No.	Coded value				SFL (kN)
	RS	PR	DT	D/d	
1	-1	-1	-1	-1	3.07
2	+1	-1	-1	-1	3.65
3	-1	+1	-1	-1	3.39
4	+1	+1	-1	-1	3.89
5	-1	-1	+1	-1	3.59
6	+1	-1	+1	-1	4.11
7	-1	+1	+1	-1	3.85
8	+1	+1	+1	-1	4.34
9	-1	-1	-1	+1	3.44
10	+1	-1	-1	+1	3.91
11	-1	+1	-1	+1	3.69
12	+1	+1	-1	+1	4.14
13	-1	-1	+1	+1	3.88
14	+1	-1	+1	+1	4.35
15	-1	+1	+1	+1	4.10
16	+1	+1	+1	+1	4.52
17	-2	0	0	0	2.99
18	+2	0	0	0	3.92
19	0	-2	0	0	3.79
20	0	+2	0	0	4.18
21	0	0	-2	0	3.44
22	0	0	+2	0	4.38
23	0	0	0	-2	3.88
24	0	0	0	+2	4.42
25	0	0	0	0	4.74
26	0	0	0	0	4.72
27	0	0	0	0	4.75
28	0	0	0	0	4.71
29	0	0	0	0	4.79
30	0	0	0	0	4.76

Table 6. Effect of rotational speed on SFL of bimetallic joints.

Sl. No	Rotational speed (rpm)	Hook geometry			Observation
		HH	HW	HI	
1	1600	1.02	0.7	1.1	SFL: 2.99 kN; FM: Eyelet; FP: cleavage.
2	1800	0.98	0.1	1.3	SFL = 3.1 kN; FM: Partially curved; FP: cleavage facet.
3	2000	0.89	1.3	1.4	SFL = 4.79 kN; FM: Nugget pull out; FP: Fine dimples.
4	2200	0.94	1.1	0.9	SFL = 3.92 kN; FM: Partially curved; FP: Fine dimples.
5	2400	1.04	0.9	1.1	SFL = 3.72 kN FM: Partially curved FP: Coarse and shear ridges

HH- Hook height "mm", HW-Hook width "mm", HI- Hook initiation distance "mm".

between top and bottom sheets and causes a reduced region of complete metallurgical bond in the weld nugget. The strength of the joint also depends on the peak temperature due to the PR and retention of torque and magnitude characterized by the hardness of the nugget zone. The cycle time variations along with the varied heat input, axial force over the spot yielded different joint strength. Some observed higher SFL for lower PR although this varied with the RS used [28]. A marginal influence of PR on joint strength has also been reported in some studies [29].

Table 7. Effect of plunge rate on SFL of bimetallic joints.

Sl. No	Plunge rate (mm/min)	Hook geometry			Observation
		HH	HW	HI	
1	5	0.87	0.77	0.77	SFL:3.79 kN; FM: Partially curved; FP: Cleavage
2	6	0.45	0.85	2.89	SFL: 4.01 kN; FM: Partially curved; FP: Cleavage.
3	7	0.32	1.39	3.2	SFL: 4.79 kN FM: Nugget pullout; FP: fine dimples.
	8	0.47	1.01	2.39	SFL:4.52 kN; FM: Partially curved; FP: Cleavage.
5	9	0.54	0.93	1.47	SFL:4.18 kN; FM: Partially curved; FP: cleavage.

HH- Hook height "mm", HW-Hook width "mm", HI- Hook initiation distance "mm".

Table 8. Effect of tool dwell time on SFL of bimetallic joints.

Sl. No	Dwell time (sec)	Hook Geometry			Observation
		HH	HW	HI	
1	15	0.45	1.21	1.01	SFL: 3.44 kN; FM: Partially curved; FP: Shear ridges
2	20	0.41	1.28	1.45	SFL:4.10 kN FM: Partially curved; FP: Cleavage.
3	25	0.35	1.37	1.91	SFL:4.79 kN FM: Nugget pullout; FP: Fine dimples.
4	30	0.36	1.12	1.86	SFL: 4.53 kN FM: Partially curved; FP: Elongated dimples.
5	35	0.58	1.01	1.75	SFL:4.38 kN FM: Partially curved; FP: Cleavage

HH- Hook height "mm", HW-Hook width "mm", HI- Hook initiation distance "mm".

Table 9. Effect of tool diameter ratio on SFL of bimetallic joints.

Sl. No	Tool diameter ratio	Hook geometry			Observation
		HH	HW	HI	
1	2.5	0.65	1.32	1.32	SFL:3.88 kN; FP: Partially curved; FP: Cleavage.
2	3.0	0.58	1.37	1.95	SFL: 4.21kN; FP: Partially curved; FP: cleavage.
3	3.5	0.48	1.41	2.12	SFL:4.79 kN, FM: Nugget pullout; FP: Fine dimple.
4	4.0	4.48	1.23	1.98	SFL:4.61 kN FP: Partially curved; FP: Shear cleavage.
5	4.5	0.51	0.98	1.78	SFL:4.42 kN FM: Partially curved; FP: Cleavage.

HH- Hook height "mm", HW-Hook width "mm", HI- Hook initiation distance "mm".

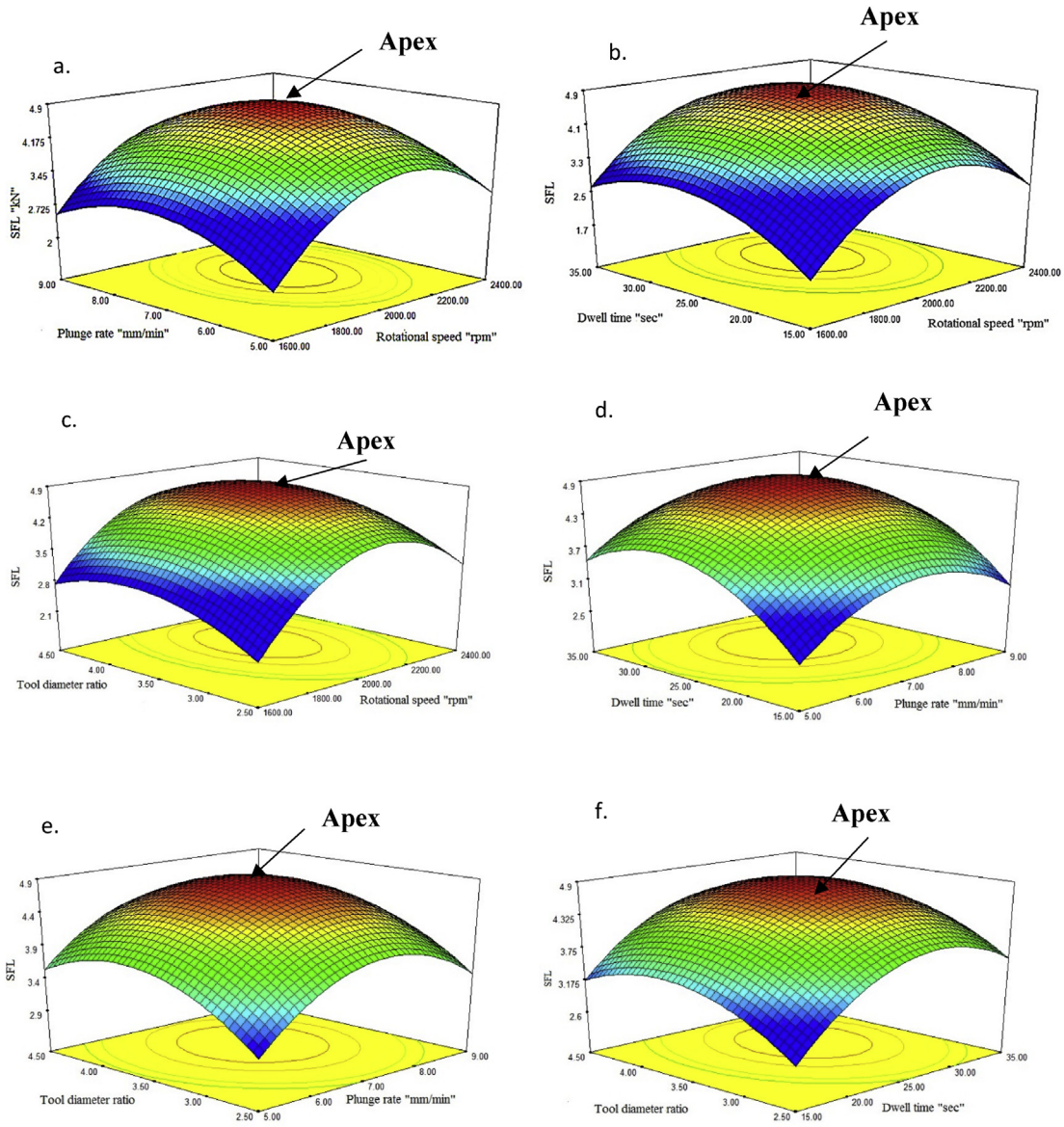

Figure 3. a-f) Effect of FSSW parameters on shear fracture load.

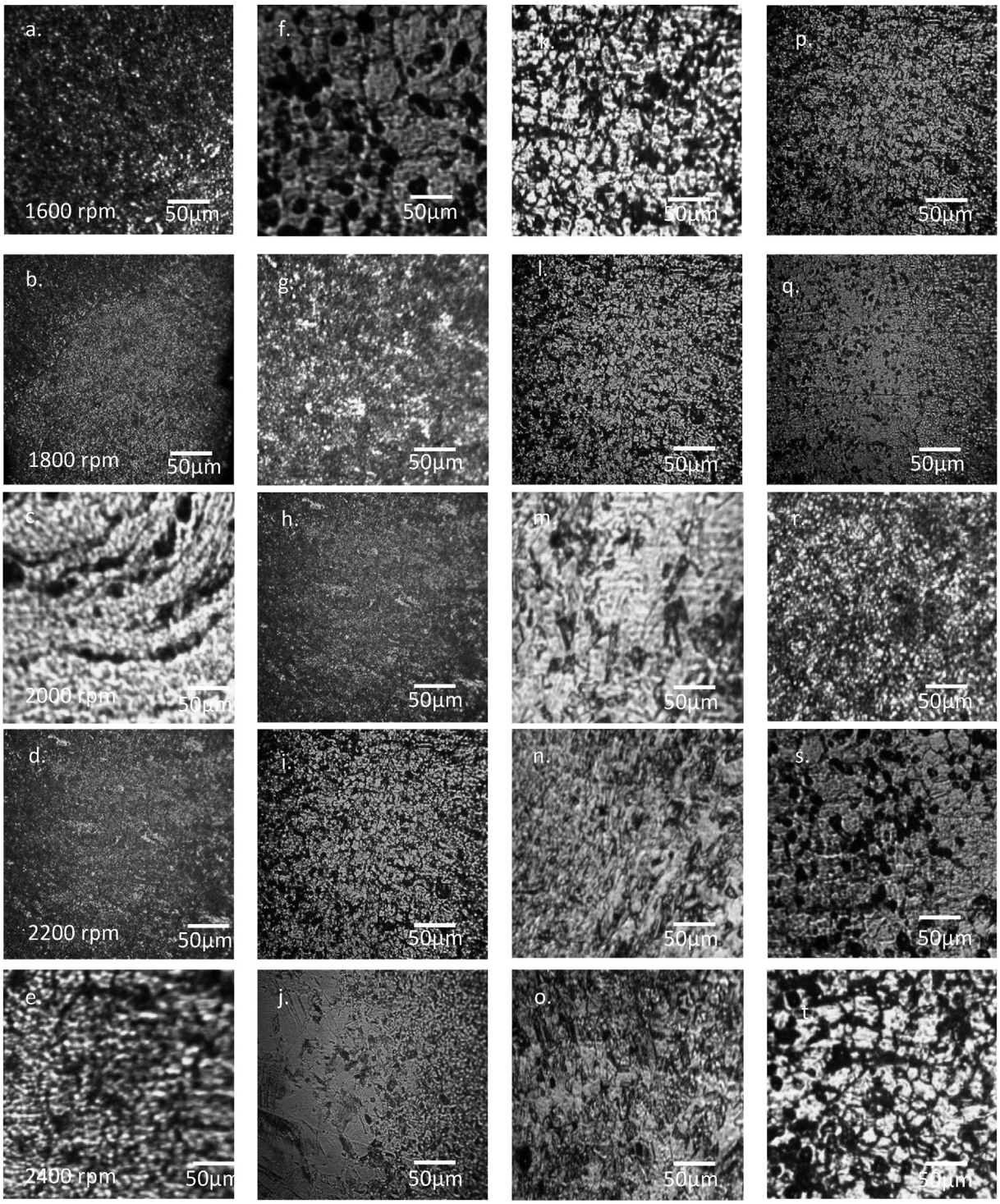

Figure 4. Micrograph of nugget zone a-e) Effect of tool rotational speed, f-j) Effect of plunge rate, k-o) Effect of dwell time, p-t) Effect of tool diameter ratio.

3.3. Effect of dwell time

Dwell time is the time for the tool to rotate to make the joint. SFL of the joints increase with increases in DT from 15 s to 25 s (Figure 3d, e). The maximum SFL of 4.79 kN were exhibited at a DT of 25 s, and the lowest SFL of 3.44kN was found at a DT of 15 s. From the macro-structural analysis (Figure 7), it is observed that increase in HW increases the SFL whereas an increase in HH decreases the SFL, irrespective of the DT. The maximum SFL was obtained in the joint fabricated using a DT of 25 s, and it possesses the optimum HW and HH of 1.37 mm and 0.35 mm respectively, whereas the minimum SFL was seen at a DT of 15 s, displaying a HW and HH of 1.21 mm and 0.456 mm respectively (Table 8). The highest nugget zone microhardness of 169 HV was measured in the joint fabricated at a DT of 25 s. The lowest nugget zone microhardness of 144 HV was recorded in the joint fabricated at a DT of 15 s. Table 8 shows the photographs of top and bottom sheet after testing and SEM fractographs. From the fracture morphology (Figure 7), it is found that the fractured surface of joint fabricated using a DT of 15 s and 20 s reveal a 'Partially Curved' mode of failure. The fractured surface of joints fabricated using a DT of 25 s exhibit 'Nugget Pull out' type of failure. It is clear that the DT has a major influence on the mode of failure of FSSW joints. The consolidated results of effect of DT. The cycle time is

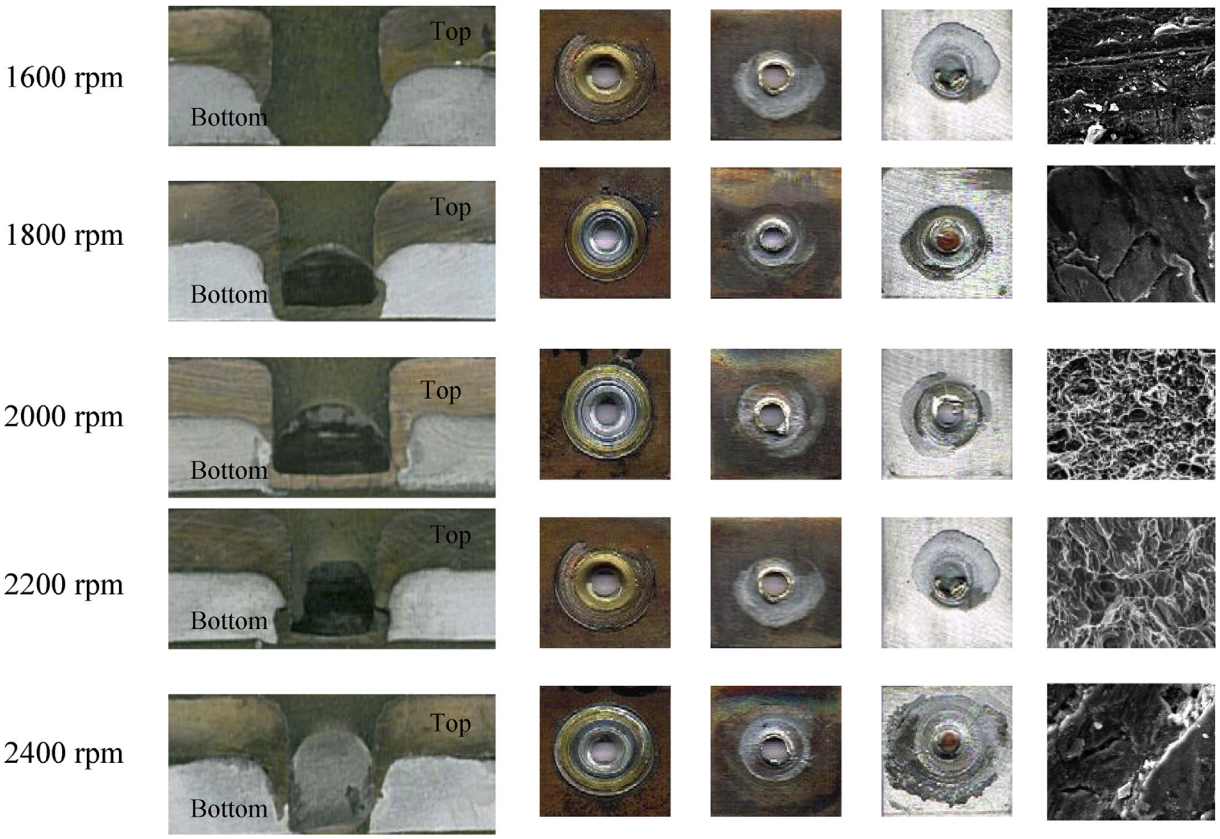

Figure 5. Effect of rotational speed on cross-section of weld, top side of top sheet, bottom side of top sheet, top side of bottom sheet and fracture surface.

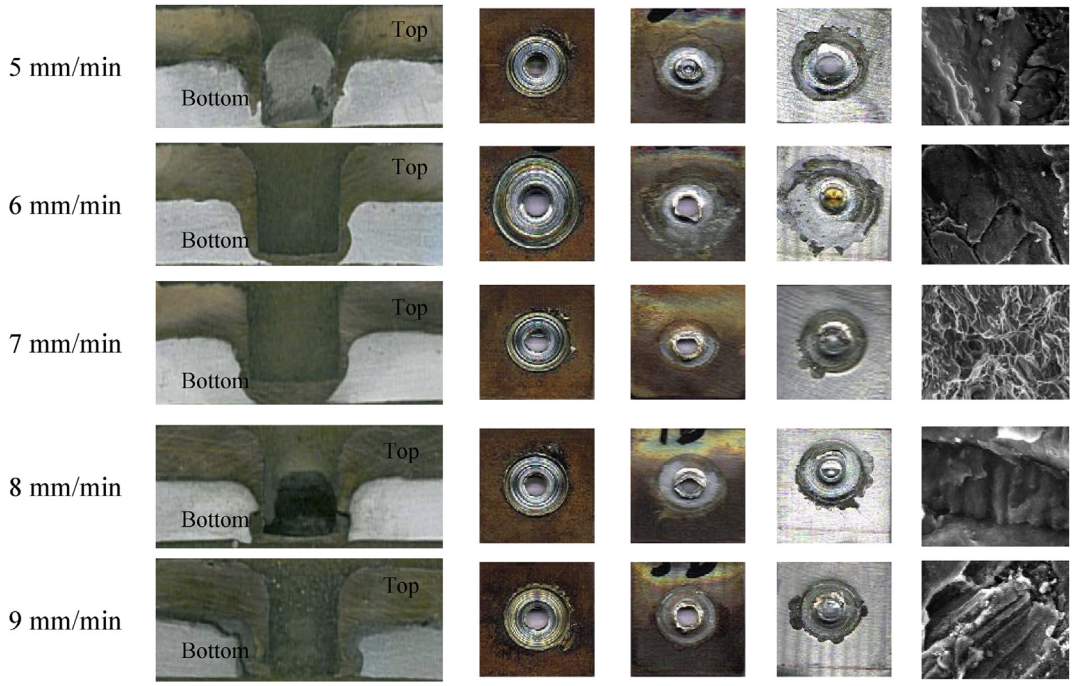

Figure 6. Effect of plunge rate on cross-section of weld, top side of top sheet, bottom side of top sheet, top side of bottom sheet and fracture surface.

increased as the DT is increased. At lower DT, the low peak temperature along with low heat input causes low stirring action (inadequate plasticization) and results in partially recrystallized structure in the nugget zone (Figure 4k). At higher DT (35 s, Figure 4o), the higher peak temperature, along with high heat input, causes excessive plasticization in the nugget zone and results in coarser grains due to slow cooling rate.

The moderately high temperatures and the duration of the axial force (Figure 4m) lead to the formation of fine grains in the nugget zone. Because of high heat input at longer DT the forging force is reduced. This

Figure 7. Effect of dwell time on cross-section of weld, top side of top sheet, bottom side of top sheet, top side of bottom sheet and fracture surface.

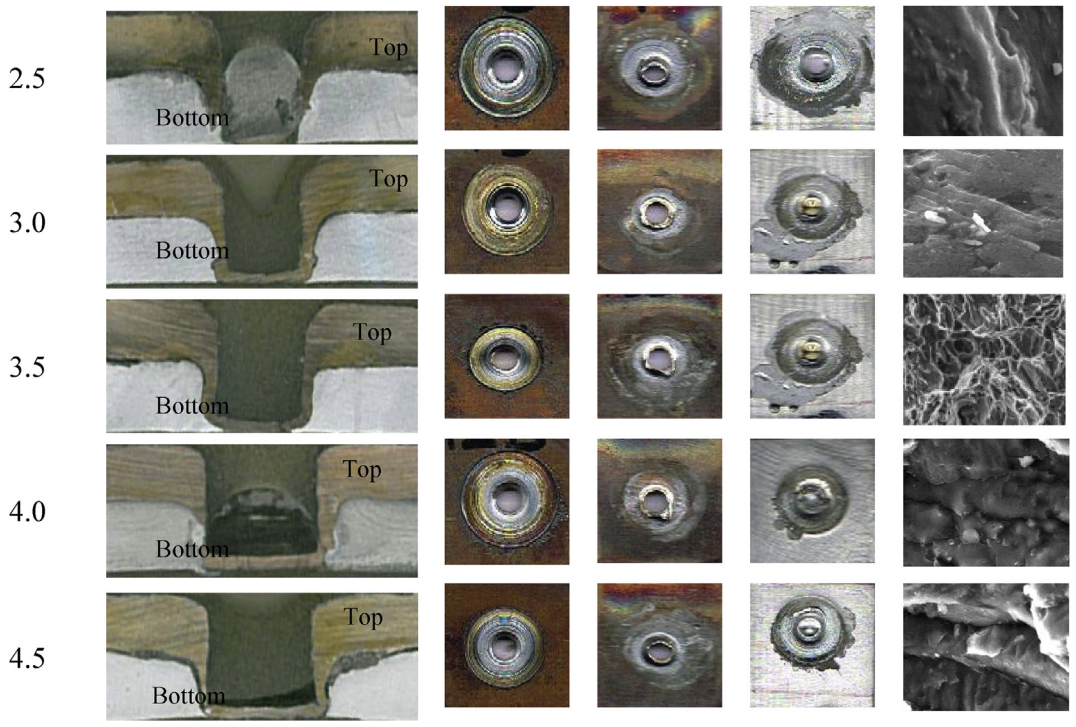

Figure 8. Effect of D/d ratio on cross-section of weld, top side of top sheet, bottom side of top sheet, top side of bottom sheet and fracture surface.

results in the poor material consolidation between top and bottom sheets; and the lower hardness at the nugget zone. An increase in tool-holding time increases the actual nugget diameter [23]. The frictional heat generated by the rotating tool imping on the upper sheet material is larger when the DT is longer. The weld diameter increases due to the larger quantum of plastic deformation near the interfacial surface, leading to increase in joint strength. It should also be found that welds were not bonded at processing times shorter than the minimum processing time of the range. Meanwhile holes were found in welds at processing time longer than the maximum processing time of the range due to high heat input in the central portion of the weld because of the highly plasticized material being pulled out by the tool during tool retraction [30].

3.4. Effect of tool diameter ratio

The SFL increases with increase in D/d from 2.5 to 3.5 and SFL decreases beyond 3.5 (Figure 3c, e, f). The highest SFL of 4.79 kN was found

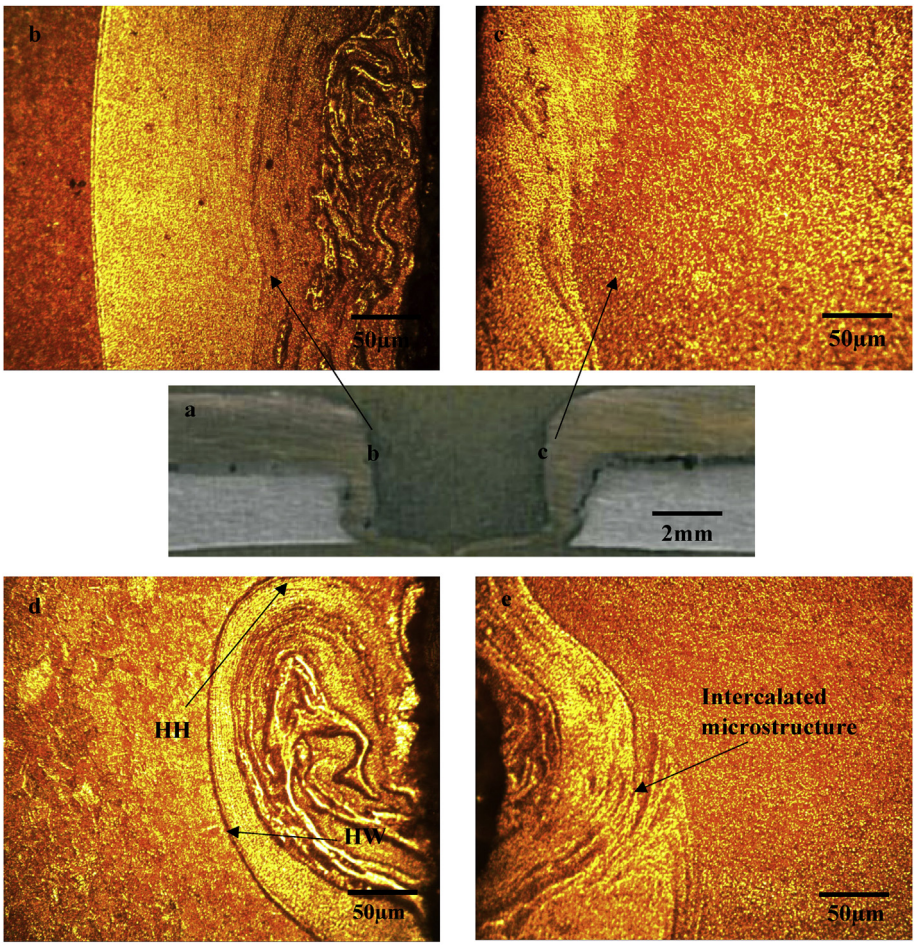

Figure 9. a) Macrograph of FSSW joint, b) Interface at TMAZ/Nugget zone on advancing side c) Interface at TMAZ/Nugget zone on retreating side, d) Magnified view of b, e) Magnified view of c.

at a D/d of 3.5. The lowest SFL of 3.88 kN was found at a D/d of 1.5. Table 9 shows the changes in geometrical features due to variations in D/d. From the macrographs (Figure 8), HH, HW and HI were measured. An increase in HW increases the SFL whereas an increase in HH decreases the SFL irrespective of the D/d. The maximum SFL was obtained by the joint fabricated using a D/d of 3.5 at an optimum HW and HH of 1.414 mm and 0.481 mm respectively. The minimum SFL was exhibited at a D/d of 2.5, where the values of HW and HW were 1.324 mm and 0.652 mm respectively. The D/d shows a significant influence on size of the grains formed at the nugget zone (Figure 4p-t), TMAZ and HAZ. Very fine grains are formed in the nugget zone at a D/d of 3.5 (Figure 4r). Grains are slightly bigger in the nugget zone of the joints fabricated at D/d other than 3.5.

From the fracture surface analysis (Figure 8), it is found that the fractured surface of the joints at a D/d of 2.5 and 3.0 reveal a 'Partially Curved' mode of failure, whereas the joint fabricated using a D/d of 3.5 exhibits 'Nugget Pull out' type of failure. The fractured surface of joint fabricated using tool diameter ratios of 4.0 and 4.5 reveal a 'Partially Curved' mode of failure. The area of the contact surface is increased as the D/d is increased. At lower D/d, the smaller contact areas generate low peak temperatures, which, along with low heat input, causes low stirring action and results in coarser grain structure in the nugget zone. At higher D/d, the higher peak temperature due to a larger contact surface, along with high heat input causes excessive plasticization and results in coarser grains in the nugget zone. It should also be noted that the excessive heat input is used only to increase the width of the HAZ, and not the volume of the nugget zone [18]. Because of high heat input at higher D/d the forging force is reduced, which results in poor material consolidation between the overlapping sheets and lower hardness at the nugget zone. The actual nugget size increases with increasing D/d. The frictional heat generated by the rotating tool impinging on the upper sheet material is also greater at higher ratios of D/d. The weld diameter is increased due to the larger plastic deformation of the sheet materials near the interfacial surface. The increased weld diameter increases the joint strength. The weld made at the D/d lower than the minimum D/d was not bonded while the weld made at the D/d greater than the maximum D/d of the range was inferior because of the highly plasticized the material.

It is also found that the increase of HW increases the SFL. However the increase in HH decreases the SFL independent of the D/d (Table 9). The HI from the tool interface of the joints, with a few exceptions, is found to increase in proportion to the increase in SFL. The contradiction in the HI is due to the volume of material thrown and thermo-mechanical effect produced by the process parameters at different D/d used during fabrication. The nugget zone width along the interface in the weld region and the nugget zone volume was dependent on the peak temperature variation resulting from the change in D/d. The variations in geometrical features depend on the process parameters, and this has resulted in a consequent change in HW, the modes of failure and the fracture values [31]. Higher Fracture loads are required for the long HW and deep effective top sheet thickness whereas lower fracture loads are sufficient for the shorter HW and shallow effective top sheet thickness. The maximum resistance to fracture along the interface through bonding region is offered by the nugget zone as its width is high, while the hook orientation influences the crack propagation. The final fracture is

completed along the shortest path of either the bonded region in lap shear tensile loading effective or the top sheet thickness [23]. When the load is applied, crack is initiated at the juncture of the the overlapping sheets, progresses to the region of mechanical bonding and propagates through metallurgical bond. The joint fails when the crack finally reaches the nugget zone. It is found that the fractures are in the mode of dimple rupture. The size of the dimples depends significantly on the process parameters used, even though the failure invariably consists of dimples and cleavage.

The difference in fracture resulted due to the difference in grain size, which is evident from the fractographs. Cleavage type of fracture was observed at lower tool rotational speed of 1600 rpm and 1800 rpm with eyelet mode and partially curved of failure, whereas fine and deep dimples are seen in nugget pullout. Fractographs of partially curved interfacial lies between eyelet and nugget pull out (Figure 8). The dimple size shows that the strength and ductility are directly proportional. The strength and ductility of the joint is higher if the dimple size is finer [32]. The plasticity is lowered significantly due to the discontinuous oxide particles present, which influence the formation of these dimples. However, the HW is the most the important geometric feature influencing crack propagation and final fracture [31]. However, the joints fractured at different loads, depending on the width of the nugget zone and the area of the faying surfaces resulting from the different process parameters.

3.5. Integrity of the FSSW joint

From the test results, it is understood the flow behavior of the material in the welds is controlled by the thermal flux. The effect of FSSW parameters on SFL have been discussed and correlated with the weld geometry such as HH, HW and nugget zone volume. The effect of individual and combined process parameters on SFL of FSSW joints are shown in Figure 3. The SFL of the joint increases with increasing RS, PR and D/d ratio to a certain level, and then decreases. The sufficient flow of materials in the nugget zone, ensured by the proper selection of FSSW parameters and tool pin geometry results in the maximum SFL. Figure 9 depicts the macro and microstructure of sound welded joints of bimetallic FSSW joints. The FSSW joints also exhibit characteristics similar to friction stir welding. The microstructure of Nugget zone is flanked by TMAZ on both sides and defect free joints can be achieved by select proper combination of FSSW parameters. The nugget zone exhibits an intercalated microstructure (Figure 9b,c). The micrograph of the advancing side TMAZ revealed elongated and downward flow of material (Figure 9d). On the other hand, an upward flow is observed on the retreating side TMAZ (Figure 9e). A uniform distribution of intermetallic compounds was observed on both sides. In Al-Cu binary system, six possible phases would occur well below 500 °C. Along the intermetallic compounds several Meta stable phases are also possible [33]. The weldability studies of AA6061 with copper alloy using FSSW, has shown that the intermetallic compound formation has reduced the strength of FSSW joints. In contrast, the continuous formation of intermetallic compounds like γ_2-Cu_9Al_4 in the Cu zone and η_2-CuAl in the Al zone has more impact on the strength [34]. This may be the reason for the joint yielding a higher SFL than other joints.

4. Conclusions

AA6061-T6 aluminum alloy was successfully welded in this investigation with copper alloy using friction stir spot welding method. The following important inferences are drawn:

(i) Friction stir spot welding was performed as per the conditions dictated in the design matrix.
(ii) The maximum SFL of 4.79 kN was found at a rotational speed of 2000 rpm, plunge rate of 7 mm/min, dwell time of 25 s and diameter ratio of 3.5.
(iii) The maximum shear fracture load of joint was achieved at an optimal hook height of 0.89 mm, hook width of 1.3 mm and hook initiation point of 1.4 mm.
(iv) The continuous formation of intermetallic compound such as γ_2-Cu_9Al_4 and η_2-CuAl in the Cu zone and the Al zone respectively may be the reason for higher shear fracture load.
(v) The fracture modes are classified in to eyelet, partially curved and nugget pull out, and result from the heat input at the vicinity,
(vi) Of the three mode of fracture, the maximum shear fracture load was obtained in the nugget pullout mode of failure.

Declarations

Author contribution statement

S. Manickam: Conceived and designed the experiments; Analyzed and interpreted the data.

C. Rajendran: Performed the experiments; Contributed reagents, materials, analysis tools or data.

V. Balasubramanian: Contributed reagents, materials, analysis tools or data; Wrote the paper.

Funding statement

This research did not receive any specific grant from funding agencies in the public, commercial, or not-for-profit sectors.

Competing interest statement

The authors declare no conflict of interest.

Additional information

No additional information is available for this paper.

References

[1] R. Karthikeyan, V. Balasubramanian, Predictions of the optimized friction stir spot welding process parameters for joining AA2024 aluminum alloy using RSM, Int. J. Adv. Manuf. Technol. 51 (2010) 173–183.
[2] V. Balasubramanian, Relationship between base metal properties and friction stir welding process parameters, Mater. Sci. Eng. 480 (2007) 397–403.
[3] U.F.H. Suhuddin, V. Fischer, J.F. dos Santos, The thermal cycle during the dissimilar friction spot welding of aluminum and magnesium alloy, Scripta Mater. 68 (1) (2013) 87–90.
[4] S.H. Chowdry, D.L. Chen, S.D. Bhole, X. Cao, P. Wanjar, Lap shear strength and fatigue behavior of friction stir spot welded dissimilar magnesium- to- aluminum joints with adhesive, Mater. Sci. Eng. 562 (2013) 53–60.
[5] Sami Sayer Uğur Özdemir, Çınar Yeni, Effect of pin penetration depth on the mechanical properties of friction stir spot welded aluminum and copper, Mater. Testing 54 (4) (2012) 233–239.
[6] R. Hedeman, C. Johnson, S. Kou, Metallurgical analysis of Al/Cu friction stir spot welding, Sci. Technol. Weld. Join. 15 (7) (2010) 597–604.
[7] Z.W. Chen, S. Yazdanian, Friction Stir Lap Welding: material flow, joint structure and strength, J. Achiev. Mater. Manufact. Eng. 55/2 (2012) 629–637.
[8] Y.F. Sun, H. Fuji, N. Takaki, Y. Okitsu, Microstructure and mechanical properties of dissimilar Al alloy/steel joints prepared by a flat spot friction stir welding technique, Mater. Des. 47 (2013) 350–357.
[9] C. Connolly, Friction spot joining in aluminum car bodies, Ind. Robot: Int. J. 34 (1) (2007) 17–20.
[10] Mazda Press Release, Mazda develops world's first steel and aluminum joining technology using friction heat, 2005. June 2, 2005.
[11] Toyota Prius, AEI Best Engineered Vehicle 2004, SAE Technical Paper, in: Automotive Engineering International, 2004, pp. 58–64.
[12] R. Sakano, K. Murakami, K. Yamashita, T. Hyoe, M. Fujimoto, M. Inuzuka, Y. Nagao, H. Kashiki, Development of spot FSW robot system for automobile body members. Proceedings of 3rd International Symposium of Friction Stir Welding, Kobe, Japan, 2001.
[13] M. Kumagai, K. Tanaka, Joint properties of friction stir spot welding in a 6000 series aluminum alloy, in: The 102nd Conference of Japan Institute of Light Metals, Sapporo, Hokkaido, Japan, 2002. Paper 124, May 17-19.
[14] M. Fujimoto, M. Inuzuka, M. Nihio, Y. Nakashima, Development of friction spot joining (report 1) - cross sectional structures of friction spot joints, in: Preprints of the National Meeting of Japan Welding Society, No. 74, 2004, pp. 4–5.

[15] T. Pan, W. Zhu, W.J. Schwartz, Spot friction welding - a new joining method for aluminum sheets, in: Proceedings of the 2005 International Automotive Body Congress, September 20-21, Ann Arbor, Michigan, 2, 2005, pp. 95–99.
[16] C. Chun, W. Chang, H. Cho, Study on friction spot joining of light metal for automotive, in: Preprints of the National Meeting of Japan Welding Society No.78, 2006. Paper # 317.
[17] P. Heurtier, M.J. Jones, C. Desrayaud, J.H. D/diver, F. Montheillet, D. Allehaux, Mechanical and thermal modeling of friction stir welding, J. Mater. Process. Technol. 171 (2006) 348–357.
[18] P. Gerlich, A. Su, T.H. North, G.J. Bendzsak, Energy utilization and generation during friction stir spot welding, Sci. Technol. Weld. Join. 11 (2) (2006) 163–169.
[19] D.A. Wang, S.C. Lee, Microstructures and failure mechanisms of friction stir spot welds of aluminum 6061-T6 sheets, J. Mater. Process. Technol. 186 (2007) 291–297.
[20] H.J. Liu, H. Fuji, M. Maeda, K. Nogi, Mechanical properties of friction stir welded joints of 1050 – H24 aluminum alloy, Sci. Technol. Weld. Join. 8 (2003) 450–454.
[21] P. Su, A. Gerlich, T.H. North, G.J. Bendzsak, Energy Generation and Nugget Zone Dimensions in Friction Stir Spot Welds, SAE Technical Paper, 2006-01-0971, SAE 2006 World Congress, Detroit, Michigan, 2006. April 3-6.
[22] S. Lathabai, M.J. Painter, G.M.D. Cantin, V.K. Tyagi, Friction spot joining of an extruded Al–Mg–Si alloy, Scripta Mater. 55 (2006) 899–902.
[23] Y. Tozaki, Y. Umematsu, K. Tokaji, Effect of processing parameters on static strength of dissimilar friction stir spot-welds between different aluminum alloys, Fatig. Fract. Eng. Mater. Struct. 30 (2007) 143–148.
[24] G. Liu, L.E. Murr, C.S. Niou, J.C. McClure, F.R. Vega, Microstructural aspects of the friction-stir welding of 6061-T6 aluminum, Scripta Mater. 37 (1997) 355–361.
[25] L.E. Murr, G. Liu, J.C. McClure, A TEM study of precipitation and related microstructures in friction-stir-welded 6061 aluminum, J. Mater. Sci. 33 (5) (1998) 1243–1251.
[26] Y. Bozukurt, S. Salman, G. Cam, Investigation of Friction Stir Spot weld of AA2024 and AA5754 Al alloy Sheets, in: 2nd International Conference of Welding Technology Exhibition, 2012, pp. 357–368.
[27] C. Genevois, A. Deschamps, A. Denquin, B. Doisneau-cottignies, Quantitative investigation of precipitation and mechanical behaviour for AA2024 friction stir welds, Acta Mater. 53 (8) (2005) 2447–2458.
[28] J.F. Henrichs, C.B. Smith, B.F. Orsini, R.J. De George, B.J. Smale, P.C. Ruehl, Friction stir welding for the 21st century automotive industry, in: Proceedings of the 5th International Symposium of Friction Stir Welding, September 14-16, Metz, France, 2004.
[29] A.C. Addison, A.J. Robelou, Friction stir spot welding: principal parameters and their effects, in: Proceedings of the 5th International Symposium of Friction Stir Welding, September 14-16, Metz, France, 2004.
[30] J. Schneider, R. Beshears, C. Arthur, J. Nunes, Interfacial sticking and slipping in the friction stir welding process, Mater. Sci. Eng. 435–436 (2006) 297–304.
[31] H. Badarinarayan, Q. Yang, S. Zhu, Effect of tool geometry on static strength of friction stir spot-welded aluminum alloy, Int. J. Mach. Tool Manufact. 49 (2) (2009) 142–148.
[32] P.C. Lin, S.H. Lin, J. Pan, T. Pan, J.M. Nicholson, M.A. Garman, Microstructures and failure mechanisms of spot friction welds in lap-shear specimens of aluminum 6111-T4 sheets, SAE Technical Paper 2004-01-1330, SAE 2004 World Congress, March 8-11, Detroit, Michigan, 2004.
[33] R. Heideman, C. Johnson, S. Kou, Metallurgical analysis of Al/Cu friction stirs spot welding, Sci. Technol. Weld. Join. 15 (7) (2010) 597–604.
[34] H. Okamura, K. Aota, Joining dissimilar materials with friction stir welding, Weld. Int. 18 (11) (2004) 852–860.